Western Kentucky University
TopSCHOLAR®

Fall 2016

Development of Dihydrochalcone Functionalized Gold Nanoparticles for Augmented Antineoplastic Activity

Jason N. Payne

Western Kentucky University, jason.payne934@topper.wku.edu

Follow this and additional works at: http://digitalcommons.wku.edu/theses

Part of the Biochemistry Commons, and the Materials Chemistry Commons

DEVELOPMENT OF DIHYDROCHALCONE FUNCTIONALIZED GOLD NANOPARTICLES FOR AUGMENTED ANTINEOPLASTIC ACTIVITY

A Thesis
Presented to
The Faculty of the Department of Chemistry
Western Kentucky University
Bowling Green, Kentucky

In Partial Fulfillment
Of the Requirements for the Degree
Master of Science

By
Jason Nathaniel Payne

December 2016

DEVELOPMENT OF DIHYDROCHALCONE FUNCTIONALIZED GOLD
NANOPARTICLES FOR AUGMENTED ANTINEOPLASTIC ACTIVITY

Date Recommended __11/7/2016__

_____
Dr. Stuart Burris, Director of Thesis

_____
Dr. Moon-Soo Kim, Thesis Reader

_____
Dr. Darwin Dahl

_____   __11/18/16__
Dean, Graduate Studies and Research   Date

ACKNOWLEDGMENTS

experience on electron microscopy; and Mrs. Alicia Pesterfield for keeping all time readiness for lab sessions and her overall support being at WKU.

Finally, I would like to thank my parents, Greg and Lisa Payne, for their support and encouragement. Having a supporting family is an invaluable asset that has made my entire post-secondary education experience all the more rewarding.

TABLE OF CONTENTS

LIST OF FIGURES

LIST OF TABLES

ABBREVIATIONS

AuNP	Gold Nanoparticles
°C	Degrees Celsius
DLS	Dynamic Light Scattering
DMEM	Dulbecco's Modified Eagle Medium
EDS	Energy Dispersive X-Ray Spectroscopy
EDTA	Ethylenediaminetetraacetic acid
FBS	Fetal Bovine Serum
FL4	Fluorescence Channel 4
g	gram
GLUT	Glucose Transporter
keV	Kiloelectronvolts
L	Liter
M	Molar
mg	Milligram
mL	Milliliter
mM	Millimolar
nm	Nanometer
PBS	Phosphate Buffer Solution
Phl-AuNP	Phloridzin Conjugated Gold Nanoparticles
Pht-AuNP	Phloretin Conjugated Gold Nanoparticles

SEM	Scanning Electron Microscopy
SGLT2	Sodium Glucose Linked Co-Transporter 2
TEM	Transmission Electron Microscopy
TGA	Thermogravimetric Analysis
µg	Microgram
µL	Microliter
ζ	Zeta Potential

DEVELOPMENT OF DIHYDROCHALCONE FUNCTIONALIZED GOLD NANOPARTICLES FOR AUGMENTED ANTINEOPLASTIC ACTIVITY

Jason Nathaniel Payne   December 2016   36 Pages

Directed by: Dr. Stuart Burris, Dr. Moon-Soo Kim, and Dr. Darwin Dahl

Department of Chemistry   Western Kentucky University

Phloridzin, an antidiabetic and antineoplastic agent usually found in fruit trees, is a dihydrochalcone constituent that has a clinical/pharmaceutical significance as a sodium-glucose linked transport 2 (SGLT2) inhibitor. Phloridzin never experienced widespread clinical usage in the pharmaceutical market due to its side effects and poor bioavailability when compared to other antidiabetic therapeutics. The poor bioavailability is primarily attributed to the degradation of the glycosidic bond of the phloridzin, resulting in the formation of phloretin, the aglycone of phloridzin and glucose. While phloretin displays a reduced capacity of SGLT2 inhibition, this nutraceutical shows enhanced antineoplastic activity in comparison to phloridzin. Gold nanoparticles (AuNPs) have been explored in improving the bioavailability of many drugs and therefore we opt for gold nanoparticle mediated delivery of phloridzin and phloretin and exploration of their anticancer mechanism. In this study, we have synthesized phloridzin and phloretin conjugated gold nanoparticles (Phl-AuNP and Pht-AuNP) in a single-step, rapid, biofriendly processes. The synthesized AuNPs morphology and elemental composition was characterized via transmission electron microscopy, UV-Vis spectroscopy, scanning electron microscopy-energy dispersive x-ray spectroscopy, and thermogravimetric analysis. Assessment of the antineoplastic potency of the dihydrochalcone-conjugated AuNPs against cancerous cell lines was accomplished through monitoring via flow cytometry. We posit that the functionalization of these chalcones onto the gold nanoparticles' surface has improved the pharmacokinetic profile of phloridzin and phloretin.

1. INTRODUCTION

As of 2016, approximately 1,685,210 individuals in the United States were diagnosed with some form of cancer[1]. This rate has been steadily increasing over the past few decades, which has led to a frantic search for effective cancer treatments. As of 2014, 1,830 drug treatments have been identified and developed[2]. This seemingly large value is inadequate and minuscule in comparison to the number of diagnosed cancer cases. Additionally, most of these treatments are derivatives of chemotherapy, which may induce significant side effects. The need for more effective treatments that can be used in combination with some less malignant treatments is of paramount importance to the medical community.

Dihydrochalcones have been established as potent compounds for a vast array of pharmaceutical applications such as antidiabetic, antifungal, anti-inflammatory, antimalarial, antibacterial and antineoplastic medications[3–7]. A dihydrochalcone pair of particular interest in this study are phloridzin (1-[2,4-dihydroxy-6-[(2S,3R,4R,5S,6R)-3,4,5-trihydroxy-6-(hydroxymethyl)tetrahydropyran-2-yl]oxy-phenyl]-3-(4-hydroxyphenyl)propan-1-one) and its aglycone, phloretin (3-(4-Hydroxyphenyl)-1-(2,4,6-trihydroxyphenyl)-1-propanone). Phloridzin was initially isolated for pharmaceutical usage as the first sodium-glucose linked transporter 2 (SGLT2) inhibitor in 1838[8,9]. The mechanism of action for phloridzin allowed for the inhibition of glucose absorption through the SGLT2 due to a binding affinity for SGLT2 that was 3000 times greater than that of glucose[9–11]. Given this mechanism, phloridzin was suggested as an appropriate treatment for hyperglycemia; however, phloridzin never achieved widespread

usage due to its poor selectivity and oral bioavailability in comparison to other drug options. The phloridzin's poor oral bioavailability is primarily attributed to the presence of lactase-phloridzin hydrolase in the microvillar membrane of the small intestine[12]. This enzyme, intended for the hydrolysis of lactose, hydrolyses the β-glycosidic bond of phloridzin, resulting in the formation of phloretin and glucose. Phloretin demonstrates more modest antidiabetic activity, in comparison to phloridzin, due to its mechanism of action, which focuses on glucose transporter (GLUT) inhibition[13]. Since phloretin's mechanism is much less specific than that of phloridzin, it is ultimately less effective for the treatment of hyperglycemia. Through comprehensive pharmaceutical experimentation, it was determined that in addition to potential pharmaceutical application of phloridzin and phloretin as an antidiabetic agent, these nutraceuticals demonstrated a significant effect as antineoplastic, antipyretic, and antimalarial agents[9,11,14,15]. Of particular interest is the potential applications of phloridzin and phloretin as antineoplastic agents. The efficacy of phloridzin and phloretin has been previously examined; it was determined that both compounds demonstrate a statistically significant antineoplastic action, where phloretin is more potent than phloridzin[5,6,16,17]. In order to properly exploit this activity to its greatest potential, a drug delivery system must be integrated with these drugs to side-step any inherent bioavailability and selectivity issues.

Nanoscale materials bring a plethora of new possibilities to medicinal chemistry. Gold nanoparticles (AuNPs) have proven to be particularly useful in medicinal chemistry due to their chemical stability, ease of surface functionalization, and relative safety, and have been used for several years for cancer drug delivery and bioimaging[18–21]. Clinically-

approved, nano-conjugated doxorubicin has demonstrated an enhanced drug accumulation and retention in multidrug resistant MCF-7/ADR cancer cells[22–26]. Provided with the highly hydroxylated structure of both phloridzin and phloretin, conjugation via hydroxyl group oxidation as an ester linkage to the AuNP structure is possible (Figure 1). These studies, among others, provide credible evidence that the conjugation of phloridzin and phloretin to AuNPs have the potential for augmented antineoplastic activity[23,26,27]. The successful conversion of an antiquated antidiabetic treatment (phloridzin) and its biodegraded precursor (phloretin) to a successful antineoplastic treatment would invigorate and revitalize such efforts, possibly leading to a new wave of effective, cost-effective antineoplastic treatments.
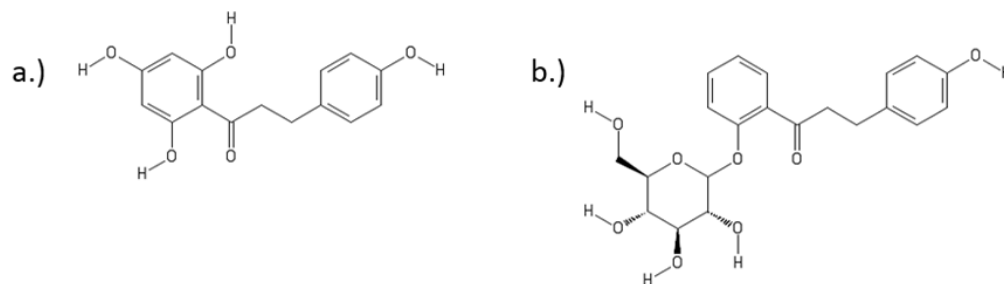
Figure 1. Chemical structures of the two dihydrochalcones. (a) phloretin molecular weight: 274.26 g mol^{-1}, (b) phloridzin molecular weight: 342.30 g mol^{-1}

2. MATERIALS AND METHODS

2.1. Materials

Chemicals	Catalog Number	Vendor
Dulbecco's modified Eagle medium	11965-092	Life Technologies
Fetal bovive serum	10437-028	Life Technologies
Formvar 15/95 resin, powder	63450-15-7	Electron Microscopy Sciences
Gold(III) chloride trihydrate	520918-5G	Sigma Aldrich
Phloretin	P7912-250MG	Sigma-Aldrich
Phloridzin dihydrate	274313-5G	Sigma-Aldrich
Potassium gold(III) chloride	450235-1G	Sigma Aldrich
Potassium phosphate, dibasic (K_2HPO_4)	PX1570-1	EMD Chemicals
Potassium phosphate, monobasic (KH_2PO_4)	PX1565-5	EMD Chemicals
Potassium sulphate	PX1595-1	EMD Chemicals
Sodium chloride	3624-05	J.T. Baker
Sodium citrate dihydrate	W302600-1KG	Sigma Aldrich
Sodium phosphate, dibasic, 12-Hydrate	SX0718-1	EMD Chemicals
SYTOX AADvanved Dead Cell Stain	1635632	Life Technologies
Trypsin-EDTA	15400054	Life Technologies

Table 1. Represents list of all the chemicals used for the research project with catalog number and vendor details respectively.

2.2. Supplies

Supply material	Catalog Number	Vendor
24-Well Flat Bottom, Non-Treated, Sterile, Polystyrene, Microtiter Plates	25381-056	Costar
Disposable Pasteur Pipets, Glass, Plugged	14672-412	VWR
Falcon Tubes – 15 mL	89039-666	VWR
Falcon Tubes – 50 mL	89004-364	VWR
Glass Culture tubes	14-961-27	Fisher brand
Microcentrifuge Tubes – 1.5 mL	87003-294	VWR
Micropipette Tips (1-1000 µL)	83007-382	VWR
Micropipette Tips (1-20 µL)	53509-070	VWR
Micropipette Tips (1-200 µL)	53503-606	VWR
Nalgene™ Oakridge High speed PPCO centrifuge tubes	3119-0030	Thermo Scientific
Sterile Polystyrene Petri Dish (100 mm x 15mm)	875713	Fisher Scientific
TEM grids (400 square mesh, Oval Hole)	G400-Cu	Electron Microscopy Sciences

Table 2. Represents list of supply material used with catalog number and vendor details respectively.

2.3. Equipment

Equipment	Application
Autoclave Machine, GETINGE	Sterilize solutions and supplies
Eppendorf Centrifuge	Concentrate gold nanoparticles (Small scale)
Excella E25 Incubator Shaker	Bacterial and nanoparticle incubation
-80 °C Freezer, Thermo scientific	Store bacterial stock culture
Hitachi U-3900 Spectrophotometer	Optical absorption of nanoparticle solution
JEOL JEM-1400 Plus Electron Microscope	Morphological characterization of kanamycin gold nanoparticles
JEOL JSM-5400 LV Scanning Microscope	Elemental composition of nanoparticles
Thermo scientific Bath Circulator (Haake A25, Haake SC150)	Temperature dependent synthesis of nanoparticles
LABONCO Biological Safety Cabinet, Logic, Class II, Type A2	Working with bacteria (aseptic conditions)
LABONCO Centrivap Cold Trap Lyophlizer	Freeze-drying of gold nanoparticles
METTLER TOLEDO New Classic MF Balance (Model: ML 54/03)	Weighing of raw materials, nanoparticles etc.
MISONIX ultrasonic Liquid Processor XL-2000 Probe Sonicator (Model: CML-4)	Break the aggregation of nanoparticles
NANOpure infinity, Ultrapure water system, Barnstead water machine	Nano pure water (17.8-18.3 mΩ-cm)
Refrigerator	Storing the solutions and reagents
SPECTRONIC 20D+ Thermo Spectronic	Determine optical density of bacteria
Sorval RC-5B/5C Plus centrifuge	Concentrate gold nanoparticles (Large scale synthesis)
TA Thermogravimetric Analysis, Q5000	Organic percent determination on gold nanoparticles
VWR Incubator	Growth of bacteria on agar plates
Zetasizer Nano S (Malvern Instruments Ltd.)	Particle size distribution

Table 3. Represents list of equipments used, their make, and uses respectively.

2.4. Preparation of reagents

2.4.1. Cleaning protocol

All the glassware/apparatus/containers were thoroughly rinsed and washed with soap water followed by tap water and nanopure water and allowed to air dry. Furthermore, the apparatus were subjected to dry heat sterilization before use.

2.4.2. Preparation of sterile nanopure water (pH 7.2 ± 0.2)

500 mL of nanopure water was collected in a sterile 1000 mL glass bottle. The cap was screwed loosely and the nanopure water was sterilized by moist heat sterilization using an autoclave at 141 °C for 75 minutes.

2.4.3. Preparation of phloretin stock solution: (0.365 M, 300 μL)

30 mg of phloretin was weighed out using a microbalance and transferred to a prepared 1.5 mL microcentrifuge tube. 300 μL of 100% ethanol was then added to the microcentrifuge tube. The tube was then thoroughly vortexed until the resultant solution was clear to ensure adequate dissolution of the phloretin in the ethanol. The phloretin stock is then divided in 30 μL aliquots in 10-50 mL falcon tubes with 30 mL of autoclaved nanopure water.

2.4.4. Preparation of phloridzin stock solution: (0.932 mM, 30 mL)

13.5 mg of phloridzin dihydrate was weighed out using a microbalance and transferred to a prepared 50 mL falcon tube. 30 mL of autoclaved nanopure water was added to the falcon tube.

2.4.5. Preparation of potassium gold (III) chloride stock solution (KAuCl$_4$) (0.79 mM, 5.0 mL)

250 mg of gold salt was weighed and transferred to 15 mL Falcon tube. 5 mL of sterile nanopure water was added to it. The mixture was vortexed to dissolve the solute until clear, homogenous yellow solution was obtained. The tube was further stored at 2-8 °C for future use.

2.4.6 Preparation of 1 mM chloroauric acid stock solution

A chloroauric acid solution was prepared by weighing out 101.94 mg on a microbalance. This was then added to a 500 mL reagent bottle, to which 300 mL of autoclaved nanopure water was added. A stir bar was inserted in the bottle and the solution was allowed to be mixed until the solution reached a homogenized pale yellow color.

2.4.7 Preparation of 1% sodium citrate dihydrate stock solution

1.000 g of sodium citrate dihydrate was weighed out on a microbalance and added it to a 250 mL bottle. To the reagent bottle, 100 mL of autoclave nanopure water was added along with a stir bar. The solution was mixed until particles were not visible.

2.4.8. Preparation of 10X phosphate buffer saline (PBS) (1L, pH 7.2 ± 0.2)

Following the cleaning protocol, 5.519 g sodium dihydrogen phosphate, 42.89 g disodium hydrogen phosphate and 87.66 g sodium chloride were weighed and transferred to 2 L Erlenmeyer flask. Approximately 800 mL of autoclaved nanopure water was added and the solutes were mixed to dissolve. The volume was made up to 1000 mL in a graduated measuring cylinder using autoclaved nanopure water. The pH of solution was

adjusted to pH 7.2 using calibrated pH meter. The 500 mL of solution was transferred to two reagent bottles, screw capped loosely and subjected to moist heat sterilization. After sterilization, the bottles were labeled, screw capped tightly and stored at room temperature until further use.

2.4.9. Preparation of 1X phosphate buffer saline (PBS) (0.5L, pH 7.2 ± 0.2)

Following the cleaning protocol, 50 mL of 10X PBS was diluted to 500 mL using autoclaved nanopure water in a graduated cylinder. The pH of solution was adjusted to pH 7.2 using calibrated pH meter. This solution was then transferred to 1 L reagent bottle, screw capped loosely and subjected to moist heat sterilization. After sterilization, the bottles were labeled, screw capped tightly and stored at room temperature until further use.

2.4.10. Preparation of 1 % formvar solution

A 1 % solution of formvar was prepared by dissolving 1 gram polyvinyl formvar desiccated resin powder in 100 mL ethylene dichloride solvent. The formvar mixture was mixed overnight in order to completely dissolve resin in solvent.

2.4.11. Preparation of TEM grids

The 400 square mesh, copper grids were obtained and washed in 1 M HCl solution in order to remove any dust particles followed by air-drying. The grids were further washed in water and air-dried. A final wash with acetone followed by air-drying was done for copper grids. The burette apparatus was set up and formvar coating solution was added into burette. A clean glass slide was dipped into the burette holding formvar solution and

kept in contact for approximately 20 seconds. The glass slide was removed using tweezer and air-dried. A surgical grade blade was used to scrap the edges of the glass slide. The film coating was then further removed from glass slide by immersing it into a glass jar completely filled with distilled water. The formvar film so obtained was deposited onto light side of washed copper grids by holding copper grids inversely (light side facing downwards) and placing it onto formvar film at surface of water. Parafilm was used to obtain formvar film containing copper grids. The copper grids (with formvar film on top) were then removed from parafilm using sharp tweezer and kept separately in a petri plate containing a filter paper.

2.5. Experimental Methods

2.5.1. Synthesis of Phloretin gold nanoparticles (Pht-AuNPs)

Phloretin has a unique solubility issue, as such it is quite soluble in aqueous media at extreme pressure or it is soluble in the presence of some organic media. To remedy this issue ethanol was used in the preparation of the phloretin stock to ensure solubility. To synthesize the Pht-AuNPs, a primary reaction mixture was prepared of 0.365 M phloretin in 100% ethanol. A secondary reaction mixture of autoclaved deionized water (pH: 7.2 ± 0.2) was preheated in a Thermo Scientific water bath at 80 °C for 20 minutes. Once adequate heating of the secondary mixture was achieved, an aliquot of the primary reaction mixture (phloretin in ethanol) was added to result in a 1.22 mM phloretin solution. This reagent mixture was removed from the water bath after the addition of the ligand, at which point an aliquot of 0.132 M $KAuCl_4$ was added to the solution to a final concentration of 0.353 mM $KAuCl_4$. After mixing, a visible colorimetric shift from

colorless to dark red was observed, indicating the formation of Pht-AuNPs. The reaction mixture was subsequently subjected to at least seven cycles of washing and centrifugation in the small-scale centrifuge (14,000 rpm for 2 hour) with autoclaved nanopure water to remove any unreacted reagents.

2.5.2 Synthesis of Phloridzin Gold Nanoparticles (Phl-AuNP)

To synthesize the Phl-AuNPs, a primary reaction mixture was prepared of 0.953 mM phloridzin in autoclaved deionized water (pH: 7.2 ± 0.2). This reagent mixture was preheated in a Thermo Scientific water bath at 90 °C for 10 minutes. Once adequate heating of the reagent mixture was achieved, an aliquot of 0.132 M $KAuCl_4$ was added to the solution to a final concentration of 1.50 mM $KAuCl_4$. This reagent mixture was removed from the water bath after the addition of the $KAuCl_4$. After mixing, a visible colorimetric shift from colorless to purple was observed, indicating the formation of Phl-AuNPs. The reaction mixture was transferred to Oakridge tubes and subsequently subjected to at least ten cycles of washing and centrifugation in the large-scale centrifuge (14,000 rpm for 20 minutes) with autoclaved deionized water to remove any unreacted reagents.

2.5.3 Synthesis of Citrate Gold Nanoparticles

The Turkevich method was employed to synthesize the citrate conjugated gold nanoparticles[28]. 200 mL of the 1 mM aurochloric acid stock was preheated to 100 °C at which point 20 mL of the 1% stock solution of sodium citrate dihydrate was added was with vigous stirring via a stir bar[29]. A colorimetric shift from colorless to dark red was observed within 10 minutes, indicative of the formation of Citrate-AuNPs. The reaction

mixture was subsequently removed from the heating source and allowed to cool to 25 °C before the solution was titrated to a pH of 7.2 ± 0.2. Unbound reactants were removed by aliquoting the solution into 15 mL falcon tubes and washing with autoclaved nanopure water and centrifugating (12,000 rpm for 20 minutes) five times.

2.5.4. Lyophilization of Pht-AuNP and Phl-AuNP

There are several advantages in lyophilizing the AuNP samples. The primary advantage is that lyophilization allows for accurate quantitative determination of the yield production, a figure that is necessary for future analysis of antineoplastic activity. Additionally this process allows the product to be stored for a greater duration of time without product degradation. For lyophilization, Pht-AuNP, Phl-AuNP, and citrate AuNP were synthesized, washed, centrifuged, and concentrated to the final volumes in multiples of 2 mL. The LABONCO Centrivap Cold Trap Lyophlizer was switched on 2 hours prior to freeze-drying to attain - 30 °C. 2 mL aliquots of AuNPs suspensions were then transferred to stainless steel cups, frozen in liquid nitrogen, and covered with miracloth, which allows loss of moisture but is not permeable for loss of AuNP. The cups were then readily transferred to the lyophilization chamber (previously cooled and maintained at - 30 °C). The chamber was closed and vacuum was switched on. The samples were kept overnight at -30 °C. The temperature was gradually increased the following day by 5 °C at 1-hour intervals between -30 °C and -5 °C, 2 hour intervals between -5 °C and 5 °C and 1 hour intervals between 5 °C and 30 °C. At 30 °C, the lyophilizer vented, switched off, and the dried Pht-AuNP, Phl-AuNP, and citrate AuNP were collected, weighed accurately and stored in a glass vial at room temperature for further analysis.

2.5.5. Characterization of Pht-AuNP and Phl-AuNP

Determination of the characteristic size, shape, and composition of the AuNP was necessary for accurate comparison of the antineoplastic activity. Various electron microscopic and spectroscopic techniques were used to confirm the presence of dihydrochalcones phloretin and phloridzin on AuNPs surfaces. Since citrate AuNP are being used as the control, the conformation of the characteristics to the importance is of the utmost importance.

UV-Vis spectroscopy (UV-Vis)

Gold nanoparticles possess a characteristic optical property, known as surface plasmon resonance (SPR).[30] This SPR band is observed in visible range of light and is dependent on the size, shape, and chemical environment in which nanoparticles are present. Hence, UV-Vis spectroscopy was used as a qualitative, analytical spectrometric technique to confirm the formation of each AuNP. A dilute suspension of each AuNP was probe sonicated for 15 seconds at 15% amplitude. UV-Vis absorption spectrum of resulting suspension was recorded in the wavelength range of 400-700 nm using a Hitachi U-3900 spectrophotometer at a resolution of 0.5 nm and scanning speed of 150 nm/min while maintaining slit width at set value of 5 nm and path length 10 mm.

Dynamic light scattering (DLS)

DLS is a rapid and accurate technique used to characterize nanoparticles suspended in liquid medium.[31] Diameter and average particle size distribution of synthesized Pht-AuNP, Phl-AuNP, and Citrate-AuNP were determined using a Zetasizer Nano S (Malvern Instruments Ltd.). For this analysis sample preparation, 1 mL of 2 mg

13

mL^{-1} AuNPs suspensions was prepared and probe sonicated. The size was reported as an average distribution for over 40 runs for each respective sample. The data obtained was plotted and average particle size distribution along with polydispersity was determined.

Transmission electron microscopy (TEM)

To characterize the morphological properties of the AuNP, such as size and shape, the samples were examined through transmission electron microscopy (TEM) using a JEOL JEM 1400Plus electron microscope operating at a 110 kV accelerating voltage. The TEM possesses high image resolution at nanometer range.[32] The TEM operate on the principle of the interaction of an electron beam with a thin specimen sample. The transmitted electrons produce a negative image of the sample on a phosphor screen, from which the size and shape of nanoparticles could be determined. Sample preparation for TEM characterization involved the placement of 10 µL of each sample suspension on formvar-coated, 400-mesh copper grids, which were allowed to air-dry for 1 hour. Images of the samples were acquired through the built-in AMT XR-81M-B camera, which were subsequently processed via the Capture Engine Software AMT Version 602.600.52.

Scanning electron microscopy-energy dispersive X-Ray spectroscopy (SEM-EDS)

Surface morphology and presence of dihydrochalcone ligands on the surface of the AuNPs was examined via the surface elemental analysis using a JEOL-JSM-6510 LV scanning electron microscope (SEM) via energy dispersive X-Ray spectroscopy (EDS) with IXRF system. For analysis, 50 µL of 1 mg mL^{-1} sonicated samples of Phl-AuNP and Pht-AuNP suspensions pipetted on a cleaned silicon wafer. The silicon chips were then spin coated and dried under vacuum at 80 °C for 2 hours. SEM images of substrates were

obtained at 20 kV accelerating voltage and 25kX magnification followed by surface elemental analysis using energy dispersive spectroscopy (EDS).

Thermogravimetric analysis (TGA)

Thermal analysis is a quantitative method used to determine the amount of organic ligand conjugated on AuNPs surface.[33] Approximately 5 mg of lyophilized AuNPs and pure phloridzin and phloretin powder was heated individually in a platinum pan supported by a highly precise microbalance. The pan was introduced into furnace chamber of the Q5000 TGA and subjected to thermal decomposition from 25 °C to 850 °C. The sample was heated at rate of 10 °C min $^{-1}$ with nitrogen (N_2) gas being used as the purge gas to a temperature of 650 °C. At this point the purge gas was switched to oxygen (O_2) gas, to facilitate complete oxidation of the organic ligands present as the temperature increased from 650 °C to 850 °C at a rate of 10 °C min $^{-1}$. The weight loss of AuNPs was monitored as a function of temperature throughout the experiment. The thermal analysis experiment of Pht-AuNP and Phl-AuNP was repeated three times to confirm the percent weight of each chalcone ligand on AuNPs' surface.

Zeta potential

Zeta potential provides a net electrical charge at the interface in colloidal system.[34] For nanoparticles suspension, measuring charge of AuNPs is a key parameter for predicting its stability and potential interactions. The electrostatic charge and stability of the nanoparticles were determined using a Zetasizer Nano S (Malvern Instruments Ltd.). 1 mg mL^{-1} AuNP suspensions were prepared by dissolving the samples in deionized water. The pH of the solution was maintained at a pH of 7.2 ± 0.2 throughout the analysis. The

analysis was performed at 25 ± 0.3 °C, at a scattering angle of 90°, and the applied voltage was 100V. Results were reported as the average of 40 measurements for each sample's ζ-potential determination[35].

2.5.6 Evaluation of Phl-AuNP and Pht-AuNP antineoplastic activity

The antineoplastic activities of Pht-AuNP and Phl-AuNP were examined against an established cancerous cell line of cervical cancer cells, HeLa cells. To establish a baseline the antineoplastic activities of pure phloridzin and phloretin were examined as well. Citrate-AuNP acted as a control group for determining the effect of AuNP on the cancerous cell given citrate-AuNP's established relativistic inert status in the literature[36,37].

Preparation of aseptic culturing conditions

The preparation of the HeLa cultures is dependent upon an aseptic environment; therefore, a proper procedure for cell culturing must be followed. All preparatory work must be performed in a LABONCO Biological Safety Cabinet, which must have the hood sash maintained at the proper position to maintain laminar airflow. Concerning the items that will be used in the hood they should all be autoclaved, this includes but not limited to: pipette tip, glass Pasteur pipettes, and 70% ethanol. The 70% ethanol will be used to sterilize all surface areas and every item that will be entering the culturing area. Finally, one must ensure that media, supplements, and reagents are sterile to prevent the growth of any microbial agents in the cell cultures.

Preparation of HeLa cell cultures

Preparation of the HeLa cell culture was split from the established HeLa cell culture strain in the Thompson Lab at the Multi-disciplinary Cancer Research Facility in the Bindley Bioscience Center at Purdue University. To accomplish this a culture media was created by adding 450 mL of DMEM with 50 mL of FBS to a sterile reagent bottle and allowing the solution to reach 25 °C in a warming bath. The trypsin-EDTA and 1X PBS must also be placed in the warming bath and be allowed to reach 25 °C. To begin splitting of the culture, the existing cell media in the petri plates in which the HeLa cells are growing must be aspirated. The HeLa cell must then be washed with 8 mL of 1X PBS, followed by immediate aspiration of the PBS. 2 mL of trypsin-EDTA was added and the plate gradually rotated to ensure that entire surface of the plate has been covered before returning the plate to the incubator for 2 minutes. 8 mL of the culture media was added to the plate upon removal from the incubator to quench the trypsinization. The 10 mL of cell was transferred into a 15 mL Falcon tube, before aliquoting 2 mL into the prepared 5-10 cm petri plate. The plates were rocked in a back and forth motion to spread to the cells evenly before adding 8 mL of culture media to the plate and incubating the plates at 37 °C, in 5% CO_2 and 95% relative humidity. The resultant HeLa cells were seeded in 24-well plates at cell densities of 75,000 cell/well.

Preparation of doped culture media

To test the antineoplastic activity of the drug conjugate AuNP and the pure form of the drug, it is necessary to devise a means through which the drug can be delivered to the cell culture. It was determined that the most efficient means of drug delivery was to dissolve the drug or drug based AuNP in the culture media and then allow the HeLa cell

to continue to growing in the media, effectively inoculating them without introducing any stress into the system. To this end stock solution of Pht-AuNP, Phl-AuNP, citrate-AuNP, phloretin, and phloridzin were all prepared at concentration of 4mg mL^{-1}, 2 mg mL^{-1}, 1 mg mL^{-1}, 0.5 mg mL^{-1}, and 0.25 mg mL^{-1}. Solvation was assured through mixing and incubation at 37 °C.

In-vitro antineoplastic assay

The determination of the augmented antineoplastic activity of the gold nanoparticle conjugated systems of phloridzin and phloretin was examined as a function of the cell viability of a population of inoculated HeLa cells over a given period. The control groups for this experiment were those of phloretin, phloridzin, and citrate-AuNP. This *in-vitro* assay relied upon the 24-well plates that were seeded after the splitting of the lab's primary HeLa cell line. After 24 hours, the culture media was replaced with the previously prepared serum-free culture media containing increasing concentrations of AuNPs and pure drugs. The plates were incubated for 1 hour and 4 hours after the inoculation with the sample culture media. After the respective incubation periods for the plates, the AuNP and pure drugs were removed via several washes with a phosphate buffer solution (pH: 7.2 ± 0.2), and fresh DMEM supplemented with 10% fetal bovine serum was added to each well. After a further incubation period of 36 hours, the media was aspirated and the cells were washed with a phosphate buffer solution. Following the wash, the cells underwent trypsinization to remove them from their plates and were then added to fluorescence-activated cell sorting tubes. To each tube 1.0 µL of Sytox 7AAD dead cell stain was added and incubated in an ice bath at 0 °C – 4 °C for 15 minutes prior to

fluorescence-activated cell sorting analysis. Fluorescence channel 4 (FL4) was used for the 7AAD fluorescence analysis. Cell viability percentage was calculated relative to the untreated cells, which were considered as 100% viability.

3. RESULTS AND DISCUSSION

3.1. Synthesis and characterization of Pht-AuNP and Phl-AuNP

The synthesis of gold nanoparticles has been traditionally, a multi-step process that relied upon the use of several chemical reagents, namely reducing agents and capping agents[21,28,29,38,39]. In general, the process of AuNP formation begins with the addition of a reducing agent to a gold salt solution, composed of gold ions (Au^{3+}/Au^{2+}), to yield reduced neutral gold atoms. These ground state gold atoms demonstrate a propensity to aggregate in a manner that results in a varied shaped, multi-faceted, polyhedron[21,40,41]. This nano-aggregate of gold atoms would expand without limit unless a capping agent is introduced into the system to limit the size, and in certain cases, the spatial dimensions[28,29,39,42]. In traditional synthesis, methodologies rely on such multi-step processes to ensure the formation of consistent and stable nanoparticles. However, such methods require additional steps for purification due to the production of reagent by-products, which ultimately result in the process having limited scalability due to its labor and material intensive nature. The methodologies employed in this synthesis procedure allow for a single-pot reaction mixture that are conveniently and completely biofriendly, which is highly desirable given the potential medicinal application of the AuNPs produced[43]. In this synthetic methodology employed, the numerous electron rich regions of both of the chalcones (phloridzin and phloretin) serve as the reducing and, ultimately, the capping

19

agent. The optimum concentration of the reagents, gold salt and phloridzin or phloretin, for AuNP synthesis was determined through assessment of the AuNP synthesis efficiency of a vast array of differing concentrations. Through these arrays, it was determined that for the optimum synthesis of phloridzin a reaction mixture of 0.953 mM phloridzin and 1.50 mM KAuCl$_4$ in water produced the optimum yield of Phl-AuNPs. In the synthesis of Pht-AuNPs, it was determined that in order to achieve adequate solvation of the potential ligand the phloretin, a 0.365 M phloretin solution in absolute ethanol must be prepared, prior to addition of phloretin to a 0.353 mM KAuCl$_4$ aqueous media (pH: 7.2 ± 0.2), yielding a 1.22 mM solution of phloretin. These synthesis strategies resulted in the high yield of Phl-AuNP and Pht-AuNP, respectively, that had stable, mostly monodispersed, and uniform morphological characteristics.

Analysis of the morphological characteristics and particle aggregation character of the Phl-AuNPs and Pht-AuNPs was accomplished through TEM analysis operating at 110kV. TEM micrographs of Phl-AuNPs revealed the nanoparticles to all be spheroid, with low amounts of aggregation, and a particle core diameter of 15 ± 5 nm (Figure 2.1(a)). Similar analysis of Pht-AuNP revealed spheroid nanoparticles that exhibited very little aggregation and a particle core diameter of 8 ± 3 nm (Figure 2.2(a)). The size and approximate shape was confirmed through analysis of the AuNPs via UV-Vis spectroscopy by exploiting the principle characteristic of metallic nanoparticles know as surface plasmon resonance (SPR). SPR is a phenomenon in which the AuNP, when exposed to an oscillating electromagnetic field in the form of light, experiences an induced oscillation of the conduction band electrons of the metallic nanoparticle[44–46]. This

oscillation of nanoparticle electrons results in a charge separation. The frequency at which the amplitude of this electron field is at its maximum is defined as the SPR and is characterized by a strong absorption of the incident light responsible for the oscillation[44,46,47]. This characteristic is dependent upon the size of the nanoparticle in question therefore through the application of spectroscopy the size of the AuNPs and their rough spatial arrangement can be estimated[48,49]. The UV-Vis spectroscopic analysis indicated peak absorptions (λmax) at 536 nm and 542 nm for Pht-AuNPs and Phl-AuNPs respectively (Figure 2.1(b) and Figure 2.2(b)). Given the presence of ligands on the AuNP core, it can be inferred that the particles are spheroid and the size is in fact in agreement with the data collected for TEM analysis[44,50]. Through the application of DLS analysis, it was possible to determine the hydrodynamic radii distribution of the AuNPs, which, unlike the TEM core diameter determination, is a measure of the particle diameter including the conjugated ligands[31]. It was determined that the hydrodynamic radii were 8 ± 2 nm and 12 ± 2 nm for Pht-AuNPs and Phl-AuNPs respectively (Figure 2.1(c) and Figure 2.2(c)).

Figure 2
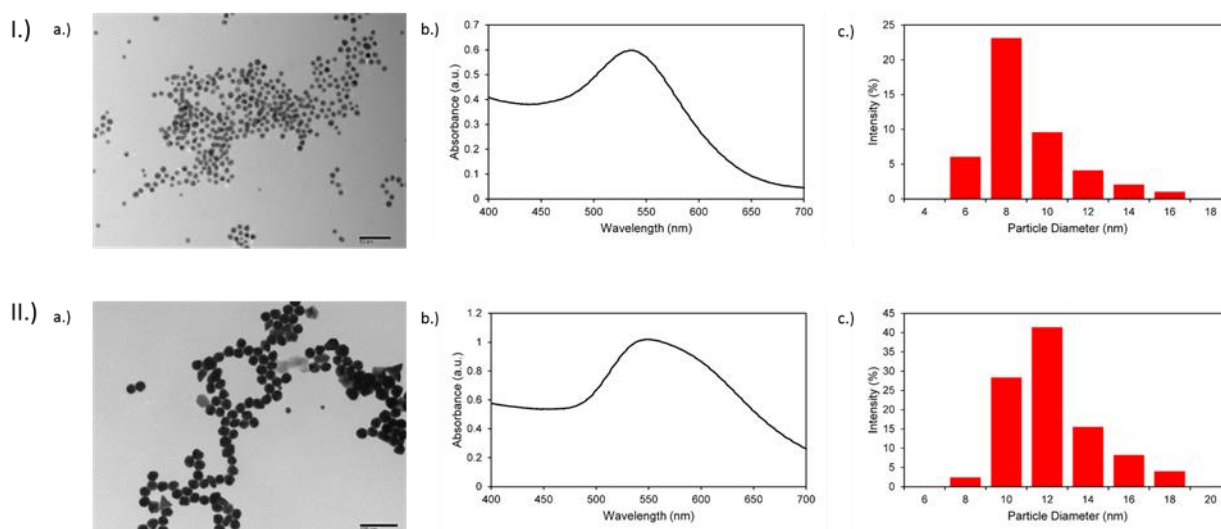
Figure 2. Illustration of the morphological and size characterization of synthesized Pht-AuNPs and Phl-AuNP through TEM, UV-Vis, and DLS analysis. I (a) TEM image showing formation of well-dispersed spherical Pht-AuNPs with a core size range of 8 ± 3 nm (scale bar= 50 nm). II (a) TEM image showing formation of well-dispersed spherical Phl-AuNPs with a core size range of 15 ± 5 nm (scale bar= 100 nm). I (b) UV-Vis spectrogram of Pht-AuNPs showing a SPR event occurring at 536 nm correlating to spheroid-shaped nanoparticles. II (b) UV-Vis spectrogram of Phl-AuNPs showing a SPR event occurring at 542 nm correlating to spheroid-shaped nanoparticles. I(c) Pht-AuNP DLS analysis shows the average hydrodynamic diameter as 8 ± 2 nm. II(c) Phl-AuNP DLS analysis depicts the average hydrodynamic diameter as 12 ± 2 nm.

22

In order to confirm the conjugation of the ligands (phloretin and phloridzin) to the nanoparticle, it was necessary to perform an elemental composition analysis. This characterization was achieved through SEM-EDS, an analytical technique that allows for the presence of carbon and oxygen to be confirmed. In this analysis the presence of both elements is confirmation of the presence of an organic ligand, specifically the drugs of interest, as the ligands are the only source of either element in the synthesis of each AuNPs. Concerning both Pht-AuNP and Phl-AuNP analysis, it was confirmed that an organic molecule was indeed present, and given the method of sample preparation for both AuNPs that organic component must correspond to the drug being conjugated to the AuNP (Figure 3.1(a) and Figure 3.2(a))[43]. Quantitative analysis of EDS spectrum produced indicated that gold accounted for 78.66% and 95.01% of the elemental composition of Pht-AuNPs and Phl-AuNPs respectively, while carbon accounted for 15.27% and 4.27% of the elemental composition of Pht-AuNP and Phl-AuNP respectively. Additionally, the oxidation state of the gold in the sample can be determined through EDS analysis depending on the shift of gold peak on the spectrogram. A position of approximately 2.120 keV corresponds to reduced gold (Au0) whereas peaks of approximately 9.712 keV corresponds to oxidized gold species (Au^{2+}/Au^{3+})[51,52]. The spectrum indicated the strong presence of gold in the reduced state, a state that is indicative of the presence of gold in a nanoparticle formation. For a quantitative elemental composition mass analysis, thermogravimetric analysis (TGA) was employed. Using this method the mass percentage composition of the organic percentage can be determined from lyophilized, powder samples ensuring that the only source of organic materials is the proposed ligands. It was

determined through the analysis that the mass percentage composition of Pht-AuNPs was 16.2% organic whereas Phl-AuNP was 4.0% organic (Figure 3.1(b) and Figure 3.2(b)). The differing mass percentages between Pht-AuNPs and Phl-AuNPs in both EDS and TGA can be accounted for due to the size of each respective ligand. Phloretin is the smaller of the two ligands as it is the aglycone of phloridzin, as such, it is to be expected that more of the smaller phloretin ligand can be conjugated to each AuNP in comparison to phloridzin. Zeta potential (ζ) analysis determined the electrokinetic potential of the AuNP samples, allowing for inference to be made regarding the stability of the AuNP in a suspension[53,54]. It was determined that the zeta potential for Pht-AuNPs was -31.7 mV (Figure 4(a)) whereas the potential for Phl-AuNPs was -38.2 mV (Figure 4(b)). In the case of both Pht-AuNP and Phl-AuNP their zeta potentials one can conclude that they demonstrate moderate stability, as the magnitude of the experimentally determined ζ is greater than 30 mV.
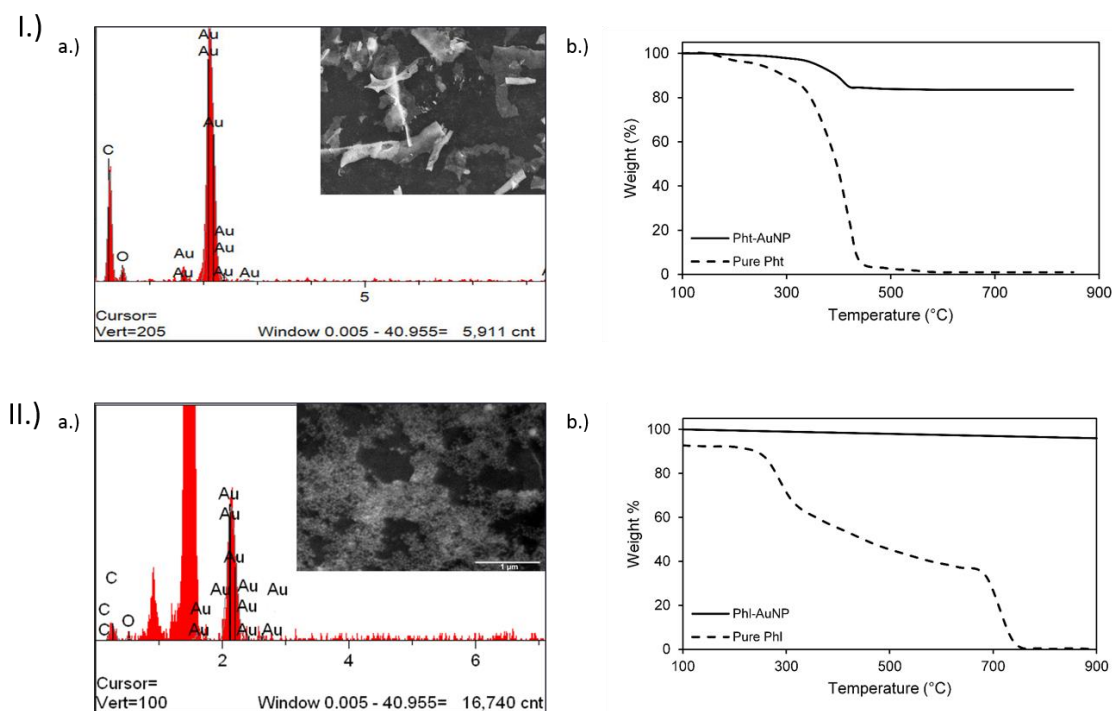
Figure 3

Figure 3: I (a) Energy dispersive spectroscopy (EDS) spectra of Pht-AuNPs showing the presence of an elemental peak for carbon (C) and gold (Au) at 0.2keV and 2.1keV respectively. Figure in the inset shows SEM image of spin coated sample of Pht-AuNPs on silicon chip obtained at an accelerating voltage of 20 keV with a magnification of 5kX. II (a) Energy dispersive spectroscopy (EDS) spectra of Pht-AuNPs showing the presence of an elemental peak for carbon (C) and gold (Au) at 0.2keV and 2.1keV respectively. Figure in the inset shows SEM image of spin coated sample of Pht-AuNPs on silicon chip obtained at an accelerating voltage of 20 keV with a magnification of 5kX. I (b) A comparison of thermo-gravimetric (TGA) analysis showing loss of organic material for Pht-AuNP (—) and phloretin (- - -) respectively. The samples were heated from room temperature to 650 °C at a rate of 10 °C min^{-1} under nitrogen flow followed by heating until 850 °C under air. II (b) A comparison of thermo-gravimetric (TGA) analysis showing loss of organic material for Phl-AuNP (—) and phloridzin (- - -) respectively. The samples were heated from room temperature to 650 °C at a rate of 10 °C min^{-1} under nitrogen flow followed by heating until 850 °C under air.
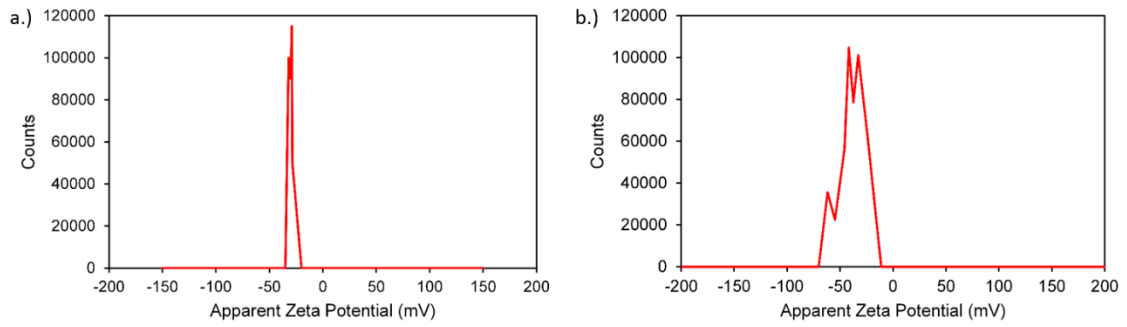
Figure 4

Figure 4. (a) Surface zeta potential analysis of Pht-AuNP determined to be -31.7mV and (b) of Phl-AuNP determined to be -38.2 mV. The magnitude of the zeta potential greater than 30 mV is indicative of a moderately stable AuNP suspension.

3.2. Evaluation of Pht-AuNP and Phl-AuNP for antineoplastic activity

The antineoplastic potentials of the synthesized Pht-AuNP and Phl-AuNP were evaluated via live/dead cell fluorescence staining assays through flow-cytometry. To perform this analysis, HeLa cells were selected to act as the model cancerous cell line. Citrate AuNPs were used as a control to evaluate the effect of the AuNP, while pure phloretin and phloridzin were used as controls to evaluate any augmented antineoplastic activity resulting from the conjugation of the drugs to the AuNP core. The efficacy of the samples was determined by the cell viability of the HeLa cells in comparison to non-inoculated HeLa cells. It was determined that inoculation times greater than 1 hour yield no statistically different cell inhibition percentages; therefore, all values represented are 1-hour post inoculation. Additionally, it was discovered that all concentrations of the samples display increasing cancerous cell cytotoxicity to a concentration of 4 mg/mL. Above 4 mg/mL, no significant increase in anticancer activity was observed. The flow-cytometry assays revealed that the pure forms of the drug ligands, phloretin and phloridzin, resulted in a HeLa cell viability of 95.000% and 88.125% respectively (Figure 5(a)). The assays that evaluated the synthesize AuNP conjugates, Pht-AuNP and Phl-AuNP, displayed a cell viability of 12.750% and 44.625%, respectively (Figure 5(b)). The efficacy of pure AuNPs was evaluated to determine if the augmented cytotoxicity was due to a synergistic effect of the conjugation or was purely due to the presence of the AuNPs. To determine the augmented synergistic potential of AuNPs, citrate-AuNPs of comparable size to the Pht-AuNP and Phl-AuNP (20 ± 5 nm) were synthesized. The surface zeta potential of the citrate-AuNPs was determined to be -33.5 mV. It was found, through

27

analysis of citrate-AuNP, that cell viability remained at 85.000% indicating the increase in toxicity was a result of a synergistic activity (Figure 5(c)). These assays demonstrate a significant increase in the cancerous cell toxicities as a result of the conjugation of the drugs to AuNPs, as indicated by the 17.45-fold increase in the efficacy of Pht-AuNPs over pure phloretin, and the 4.49-fold increase in efficacy of Phl-AuNP over pure phloridzin.

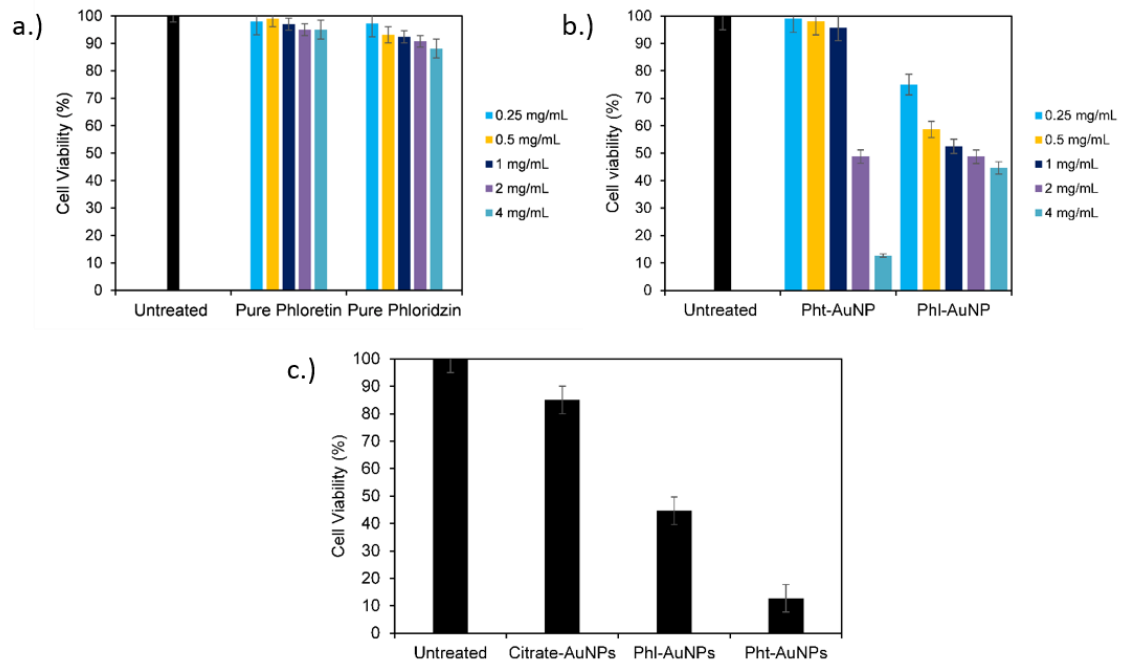**Figure 5**

Figure 5. HeLa live/dead cell fluorescence staining analysis via flow-cytometry. (a) Comparison of the pure drug forms of phloretin and phloridzin to non-inoculated cells. (b) Comparison of the AuNP functionalized forms of the drugs to non-inoculated cells. (c) Comparison of the functionalized AuNP to pure AuNP to determine the synergistic activity of the Pht-AuNP and Phl-AuNP.

4. CONCLUSION

The results concerning the functionalization of the dihydrochalcones, phloretin and phloridzin, to AuNP in an effort to augment the existing antineoplastic activity of each pharmaceutical agent reveal a potential treatment application. The functionalized AuNPs were synthesized via a single-step method that relied only upon the redox potential of the conjugate itself and required no toxic chemicals. The synthesized Phl-AuNPs were found to be in the size range of 15 ± 5 nm, whereas the Pht-AuNP were found to be 8 ± 3 nm, placing both AuNP conjugated well within the size range necessary for successful pharmaceutical applications. Significant multi-fold increases in the antineoplastic activity of both phloretin and phloridzin were observed upon the functionalization of the pharmaceutical agents to AuNPs in comparison to their pure drug forms. Evaluation of the antineoplastic of non-functionalized AuNP in conjunction with this data revealed that the augmented antineoplastic activity was in fact a result of a synergistic effect between the AuNP and each of the respective drugs. In conclusion, we report a simple, bio-friendly process using the reducing and capping potential of the dihydrochalcones, phloridzin and phloretin, to synthesize stable AuNP that have promising futures as potential antineoplastic agents.

5. FUTURE STUDIES

Mechanistic Studies of Pht-AuNP and Phl-AuNP Mode of Action

Future studies will focus on the antineoplastic mechanism of action of which phloretin and phloridzin. Previous studies have suggested that this mechanism is linked to the glucose-6-phosphate pathway or the inhibiting of DNA topoisomerases therefore that will be an area of interest[55–57]. Furthermore, the mechanism of the synergistic effect between both phloridzin and phloretin and the AuNP resulting in an augmented antineoplastic effect must be furthered studied. While a rudimentary understanding is being developed between ligands and AuNP in other applications due to the "electron sink effect" that phenomenon would seem not to apply here and thus open the possibility for a wide area of study[58].

***In vivo* interaction of Pht-AuNP and Phl-AuNP in animal model**

In order to use a nano-formulation for biological applications, the Pht-AuNP and Phl-AuNP should be tested for *in vivo* activity in experimental animal models. This will be done by studying the physiological changes occurring in animal systems upon acute and chronic exposure to Pht-AuNP and Phl-AuNP.[51] A concentration of the dihydrochalcone AuNPs will be administered intravenously to the experimental animal model and animals will be studied for various parameters such as change in body temperature, body weight and behavior before and after treatment with each AuNP.[51] The blood and urine samples will be collected at specific time intervals and tested for hematological and urinary analysis. For detailed interaction studies, serum biochemical

and histo-pathological analysis will also be done.[51] All the toxicity analysis will be done

for both AuNPs and will be compared with their respective pure drug forms.

6. REFERENCES

(1)   National Cancer Institute. NIH National Cancer Institute Cancer Statisitics. 2016.

(2)   National Cancer Institute. SEER*Rx Interactive Antineoplastic Drugs Database. 2014.

(3)   Lesse, W. I. Ueber Diabetes Bei Frauen. *Monatsschrift Für Geburtshilfe Gynäkol.* **1902**, *15* (4), 680–693.

(4)   Norton, L.; Instructor; DeFronzo, R. A.; Professor of Medicine and Chief; Abdul-Ghani, M. A.; Assistant Professor of Medicine, Division of Diabetes, University of Texas Health Science Center at San Antonio. Sodium–Glucose Co-Transporter 2 Inhibition – A Novel Strategy for Glucose Control in Type 2 Diabetes. *Eur. Endocrinol.* **2010**, *7* (1), 30.

(5)   Nelson, J. A.; Falk, R. E. The Efficacy of Phloridzin and Phloretin on Tumor Cell Growth. *Anticancer Res.* **1993**, *13* (6A), 2287–2292.

(6)   Nelson, J. A.; Falk, R. E. Phloridzin and Phloretin Inhibition of 2-Deoxy-D-Glucose Uptake by Tumor Cells in Vitro and in Vivo. *Anticancer Res.* **1993**, *13* (6A), 2293–2299.

(7)   Nakamura, Y.; Watanabe, S.; Miyake, N.; Kohno, H.; Osawa, T. Dihydrochalcones: Evaluation as Novel Radical Scavenging Antioxidants. *J. Agric. Food Chem.* **2003**, *51* (11), 3309–3312.

(8)   Stas, J. S. Ueber das Phloridzin. *J. F�r Prakt. Chem.* **1839**, *17* (1), 273–298.

(9)   Ehrenkranz, J. R. L.; Lewis, N. G.; Ronald Kahn, C.; Roth, J. Phlorizin: A Review. *Diabetes Metab. Res. Rev.* **2005**, *21* (1), 31–38.

(10)   Vick, H.; Diedrich, D. F.; Baumann, K. Reevaluation of Renal Tubular Glucose Transport Inhibition by Phlorizin Analogs. *Am. J. Physiol.* **1973**, *224* (3), 552–557.

(11)   Biegeleisen, H. Phlorizin Analogues and Their Use. US3523937 A, August 11, 1970.

(12)   Wüthrich, M.; Sterchi, E. E. Human Lactase-Phlorizin Hydrolase Expressed in COS-1 Cells Is Proteolytically Processed by the Lysosomal Pathway. *FEBS Lett.* **1997**, *405* (3), 321–327.

(13)   Lefevre, P. G. Sugar Transport in the Red Blood Cell: Structure-Activity Relationships in Substrates and Antagonists. *Pharmacol. Rev.* **1961**, *13*, 39–70.

(14)   Petersen, C. Analyse Des Phloridzins. *Ann. Acad. Sci. Francaise* **1835**, *15*, 178.

(15)   de Koninck, L. Observations Sur Les Proprietes Febrifuges de Las Phloridzine. *Bull. Soc. Sci. Medicales* **1836**, *1*, 75–110.

(16)   Wang, L.; Li, Z.-W.; Zhang, W.; Xu, R.; Gao, F.; Liu, Y.-F.; Li, Y.-J. Synthesis, Crystal Structure, and Biological Evaluation of a Series of Phloretin Derivatives. *Molecules* **2014**, *19* (10), 16447–16457.

(17)   Crespy, V.; Aprikian, O.; Morand, C.; Besson, C.; Manach, C.; Demigné, C.; Rémésy, C. Bioavailability of Phloretin and Phloridzin in Rats. *J. Nutr.* **2001**, *131* (12), 3227–3230.

(18) You, J.-O.; Guo, P.; Auguste, D. T. A Drug-Delivery Vehicle Combining the Targeting and Thermal Ablation of HER2+ Breast-Cancer Cells with Triggered Drug Release. *Angew. Chem. Int. Ed.* **2013**, *52* (15), 4141–4146.

(19) Zhou, Y.; Kong, Y.; Kundu, S.; Cirillo, J. D.; Liang, H. Antibacterial Activities of Gold and Silver Nanoparticles against Escherichia Coli and Bacillus Calmette-Guérin. *J. Nanobiotechnology* **2012**, *10* (1), 19.

(20) Seil, J. T.; Webster, T. J. Antimicrobial Applications of Nanotechnology: Methods and Literature. *Int. J. Nanomedicine* **2012**, *7*, 2767–2781.

(21) Shah, M.; Badwaik, V. D.; Dakshinamurthy, R. Biological Applications of Gold Nanoparticles. *J. Nanosci. Nanotechnol.* **2014**, *14* (1), 344–362.

(22) Zhang, L.; Gu, F.; Chan, J.; Wang, A.; Langer, R.; Farokhzad, O. Nanoparticles in Medicine: Therapeutic Applications and Developments. *Clin. Pharmacol. 38 Ther.* **2008**, *83* (5), 761–769.

(23) Aryal, S.; Grailer, J. J.; Pilla, S.; Steeber, D. A.; Gong, S. Doxorubicin Conjugated Gold Nanoparticles as Water-Soluble and pH-Responsive Anticancer Drug Nanocarriers. *J. Mater. Chem.* **2009**, *19* (42), 7879.

(24) Gu, Y.-J.; Cheng, J.; Man, C. W.-Y.; Wong, W.-T.; Cheng, S. H. Gold-Doxorubicin Nanoconjugates for Overcoming Multidrug Resistance. *Nanomedicine Nanotechnol. Biol. Med.* **2012**, *8* (2), 204–211.

(25) Prabaharan, M.; Grailer, J. J.; Pilla, S.; Steeber, D. A.; Gong, S. Gold Nanoparticles with a Monolayer of Doxorubicin-Conjugated Amphiphilic Block Copolymer for Tumor-Targeted Drug Delivery. *Biomaterials* **2009**, *30* (30), 6065–6075.

(26) Wang, F.; Wang, Y.-C.; Dou, S.; Xiong, M.-H.; Sun, T.-M.; Wang, J. Doxorubicin-Tethered Responsive Gold Nanoparticles Facilitate Intracellular Drug Delivery for Overcoming Multidrug Resistance in Cancer Cells. *ACS Nano* **2011**, *5* (5), 3679–3692.

(27) Brown, S. D.; Nativo, P.; Smith, J.-A.; Stirling, D.; Edwards, P. R.; Venugopal, B.; Flint, D. J.; Plumb, J. A.; Graham, D.; Wheate, N. J. Gold Nanoparticles for the Improved Anticancer Drug Delivery of the Active Component of Oxaliplatin. *J. Am. Chem. Soc.* **2010**, *132* (13), 4678–4684.

(28) Turkevich, J.; Stevenson, P. C.; Hillier, J. A Study of the Nucleation and Growth Processes in the Synthesis of Colloidal Gold. *Discuss. Faraday Soc.* **1951**, *11*, 55.

(29) Kimling, J.; Maier, M.; Okenve, B.; Kotaidis, V.; Ballot, H.; Plech, A. Turkevich Method for Gold Nanoparticle Synthesis Revisited. *J. Phys. Chem. B* **2006**, *110* (32), 15700–15707.

(30) Hutter, E.; Fendler, J. H. Exploitation of Localized Surface Plasmon Resonance. *Adv. Mater.* **2004**, *16* (19), 1685–1706.

(31) Khlebtsov, B. N.; Khlebtsov, N. G. On the Measurement of Gold Nanoparticle Sizes by the Dynamic Light Scattering Method. *Colloid J.* **2011**, *73* (1), 118–127.

(32) S. Pender, D.; M. Vangala, L.; D. Badwaik, V.; Thompson, H.; Paripelly, R.; Dakshinamurthy, R. A New Class of Gold Nanoantibiotics- Direct Coating of Ampicillin on Gold Nanoparticles. *Pharm. Nanotechnol.* **2013**, *1* (2), 126–135.

(33) Demurtas, M.; Perry, C. C. Facile One-Pot Synthesis of Amoxicillin-Coated Gold Nanoparticles and Their Antimicrobial Activity. *Gold Bull.* **2013**, *47* (1–2), 103–107.

(34) Gold Nanoparticles: Weakly Charged Cationic Nanoparticles Induce DNA Bending and Strand Separation. *Adv. Mater.* **2012**, *24* (31), 4261–4265.

(35) Nanotechnology Characterization Laboratory. *Measuring Zeta Potential of Nanoparticles, NCL Method PCC-2*; National Cancer Institute-Frederick: Frederick, MD, 2009.

(36) Jeerage, K. M.; Oreskovic, T. L.; Curtin, A. E.; Sanders, A. W.; Schwindt, R. K.; Chiaramonti, A. N. Citrate-Stabilized Gold Nanoparticles as Negative Controls for Measurements of Neurite Outgrowth. *Toxicol. In Vitro* **2015**, *29* (1), 187–194.

(37) Payne, J. N.; Waghwani, H. K.; Connor, M. G.; Hamilton, W.; Tockstein, S.; Moolani, H.; Chavda, F.; Badwaik, V.; Lawrenz, M. B.; Dakshinamurthy, R. Novel Synthesis of Kanamycin Conjugated Gold Nanoparticles with Potent Antibacterial Activity. *Front. Microbiol.* **2016**, *7*.

(38) Brust, M.; Walker, M.; Bethell, D.; Schiffrin, D. J.; Whyman, R. Synthesis of Thiol-Derivatised Gold Nanoparticles in a Two-Phase Liquid?Liquid System. *J. Chem. Soc. Chem. Commun.* **1994**, No. 7, 801.

(39) Hutchings, G. J.; Brust, M.; Schmidbaur, H. Gold—an Introductory Perspective. *Chem. Soc. Rev.* **2008**, *37* (9), 1759.

(40) *Handbook of Nanobiomedical Research: Fundamentals, Applications, and Recent Developments*; Torchilin, V. P., Ed.; Frontiers in nanobiomedical research; World Scientific: [Hackensack,] New Jersey, 2014.

(41) Perala, S. R. K.; Kumar, S. On the Mechanism of Metal Nanoparticle Synthesis in the Brust–Schiffrin Method. *Langmuir* **2013**, *29* (31), 9863–9873.

(42) Navarro, J. R. G.; Lerouge, F.; Cepraga, C.; Micouin, G.; Favier, A.; Chateau, D.; Charreyre, M.-T.; Lanoë, P.-H.; Monnereau, C.; Chaput, F.; Marotte, S.; Leverrier, Y.; Marvel, J.; Kamada, K.; Andraud, C.; Baldeck, P. L.; Parola, S. Nanocarriers with Ultrahigh Chromophore Loading for Fluorescence Bio-Imaging and Photodynamic Therapy. *Biomaterials* **2013**, *34* (33), 8344–8351.

(43) Dakshinamurthy, R.; Sahi, S. Monodisperse Gold Nanoparticles and Facile, Environmentally Favorable Process for Their Manufacture. US8257670 B1, September 4, 2012.

(44) Huang, X.; El-Sayed, M. A. Gold Nanoparticles: Optical Properties and Implementations in Cancer Diagnosis and Photothermal Therapy. *J. Adv. Res.* **2010**, *1* (1), 13–28.

(45) Mie, G. Contributions to the Optics of Turbid Media, Particularly of Colloidal Metal Solutions. *Ann. Phys.* **1908**, *25* (3), 377–445.

(46) Kreibig, U.; Vollmer, M. *Optical Properties of Metal Clusters*; Toennies, J. P., Gonser, U., Osgood, R. M., Panish, M. B., Sakaki, H., Lotsch, H. K. V., Series Eds.; Springer Series in Materials Science; Springer Berlin Heidelberg: Berlin, Heidelberg, 1995; Vol. 25.

(47) Papavassiliou, G. C. Optical Properties of Small Inorganic and Organic Metal Particles. *Prog. Solid State Chem.* **1979**, *12* (3–4), 185–271.

(48) Jain, P. K.; Lee, K. S.; El-Sayed, I. H.; El-Sayed, M. A. Calculated Absorption and Scattering Properties of Gold Nanoparticles of Different Size, Shape, and Composition: Applications in Biological Imaging and Biomedicine. *J. Phys. Chem. B* **2006**, *110* (14), 7238–7248.

(49) Huang, X.; Jain, P. K.; El-Sayed, I. H.; El-Sayed, M. A. Gold Nanoparticles: Interesting Optical Properties and Recent Applications in Cancer Diagnostics and Therapy. *Nanomed.* **2007**, *2* (5), 681–693.

(50) Ali, M. E.; Hashim, U.; Mustafa, S.; Che Man, Y. B.; Islam, K. N. Gold Nanoparticle Sensor for the Visual Detection of Pork Adulteration in Meatball Formulation. *J. Nanomater.* **2012**, *2012*, 1–7.

(51) Grieken, R. E. van. *Handbook of X-Ray Spectrometry*; Marcel Dekker: New York, 2002.

(52) Badwaik, V. D.; Bartonojo, J. J.; Evans, J. W.; Sahi, S. V.; Willis, C. B.; Dakshinamurthy, R. Single-Step Biofriendly Synthesis of Surface Modifiable, near-Spherical Gold Nanoparticles for Applications in Biological Detection and Catalysis. *Langmuir ACS J. Surf. Colloids* **2011**, *27* (9), 5549–5554.

(53) Greenwood, R. Review of the Measurement of Zeta Potentials in Concentrated Aqueous Suspensions Using Electroacoustics. *Adv. Colloid Interface Sci.* **2003**, *106* (1–3), 55–81.

(54) O'Brien, R. W.; Midmore, B. R.; Lamb, A.; Hunter, R. J. Electroacoustic Studies of Moderately Concentrated Colloidal Suspensions. *Faraday Discuss. Chem. Soc.* **1990**, *90*, 301.

(55) Nair, S. V. G.; Ziaullah; Rupasinghe, H. P. V. Fatty Acid Esters of Phloridzin Induce Apoptosis of Human Liver Cancer Cells through Altered Gene Expression. *PLoS ONE* **2014**, *9* (9), e107149.

(56) Bissinger, R.; Fischer, S.; Jilani, K.; Lang, F. Stimulation of Erythrocyte Death by Phloretin. *Cell. Physiol. Biochem.* **2014**, *34* (6), 2256–2265.

(57) Shao, X.; Bai, N.; He, K.; Ho, C.-T.; Yang, C. S.; Sang, S. Apple Polyphenols, Phloretin and Phloridzin: New Trapping Agents of Reactive Dicarbonyl Species. *Chem. Res. Toxicol.* **2008**, *21* (10), 2042–2050.

(58) Li, J.; Zhou, H.; Qian, S.; Liu, Z.; Feng, J.; Jin, P.; Liu, X. Plasmonic Gold Nanoparticles Modified Titania Nanotubes for Antibacterial Application. *Appl. Phys. Lett.* **2014**, *104* (26), 261110.

(59) In Vivo PK/PD Studies | Nanomedicines Characterization Core Facility.